Virtual human modeling from photographs for garment industry

Charlie C.L.Wang* **Yu Wang** **Terry K.K.Chang** **Matthew M.F.Yuen**

Department of Mechanical Engineering, Hong Kong University of Science and Technology,

Clear Water Bay, Kowloon, Hong Kong

Abstract

The research presented in this paper is to develop a technique of virtual human modeling for the garment industry from two photographs of a human body in two orthogonal views. Firstly, an efficient segmentation method is applied on the two photographs to obtain the contours of the human body. After that, a template-based feature extraction algorithm is introduced to determine the feature points on the human contours by human morphology rules. Finally, a view-dependent deformation technique is described to construct the virtual human body by using human contours. Our segmentation algorithm is derived from the Mumford-Shah segmentation technology and the level set formulation, and it is accelerated by applying multi-pyramid levels. The deformation technique is related to axial deformation. With our deformation method, the reference silhouettes (the front-view and right-view silhouettes of the template human model) and the target silhouettes (the front-view and right-view silhouettes of the human body from the photographs) are used to deform the template human model, which is represented by a polygonal mesh with predefined features. The self-intersection problem in the axial deformation is solved in our deformation approach. Compared with other virtual human modeling approaches, the speed of constructing the human model is increased; and our deformation technique has better continuity and local deformation properties. At the end of the paper, some potential applications for the garment industry are given to demonstrate the functionality of virtual human models constructed by our approach.

Keywords: multi-pyramid segmentation, view-dependent deformation, virtual human, photograph, garment industry.

1. Introduction

The work presented in this paper comes from the project of developing a computer aided 3D pattern making platform. Such a platform is important to help apparel enterprises stay ahead of current technological

* Corresponding Author: Charlie C. L. Wang; E-mail: wangcl@ust.hk or mewangcl@hotmail.com; Tel: (852) 2358-8095

innovations by major retailers and manufacturers. Several papers about building a geometrical model by reverse engineering (RE) have been published [1, 2, 3, 4]. In RE systems, the geometric model of an object is generated from a cloud of points, which can be obtained by coordinate measuring machines (CMM) and 3D laser scanners. The accuracy of the models generated from cloudy points is always high. However, their speed is always slow. In the garment industry, sometimes, a rapid and low-cost 3D virtual human construction approach is required. For example, if a client orders custom-fitting clothes over the Internet, only the traditional tape-measurement number is not enough for the modern 3D customized pattern making (e.g., the crotch shape and orientation cannot be provided); if he has difficulty in finding a nearby service center to take a body scan, photographs of him wearing tight clothes are alternative input to solve this problem. Some research has recently generated virtual human models from photographs [5, 6]. Our method also constructs virtual human models from photographs, but the speed of human model construction is increased, the feature points on silhouettes are extracted automatically, and the continuity and the local deformation properties of our deformation are enhanced. The height of the human body is used as the parameter for the calibration.

In our approach, an efficient segmentation method is applied to two photographs (front-view and right view) to obtain the contours of the human body separately. Then, the features on the human contours are extracted based on general human knowledge (in this step, some information is transferred between the extraction of two contours). Finally, the view-dependent deformation deforms the template human model with reference to the correspondence between the reference silhouettes (the front-view and right-view silhouettes of the template human model) and the target silhouettes (the front-view and right-view silhouettes of the human from the photographs) to obtain the final human model, which is represented by a polygonal mesh. The flow chart of the whole system is shown in Fig. 1.

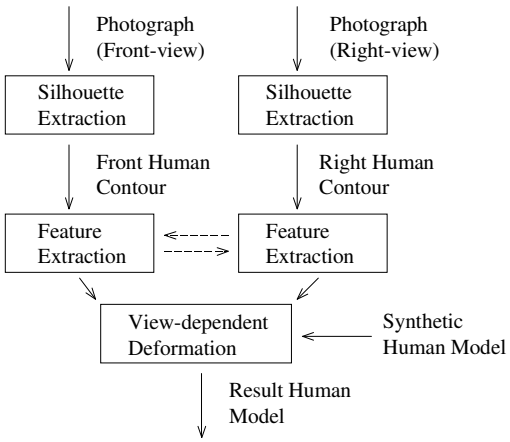

Fig. 1 Flow chart

At the end of our paper, in order to demonstrate the functionality of the virtual human models constructed by our approach, some potential applications for the garment industry are given. They are: 1) dimensions extraction from human models; 2) rapid prototyping for mannequin manufacturing; and 3) three-dimensional garment construction.

2. Related Work

Since rapid and low-cost virtual human construction approaches are sometimes required in the garment industry, some researchers recently tried to generate a virtual human model from photographs. Hilton et al. [5] introduced a technique for automatically building recognizable, moving 3D models of individuals. In their method, a set of multi-view color images of a person is captured from the front, sides and back by one or more cameras. A model based on the reconstruction of shape from silhouettes is used to transform a standard 3D generic humanoid model to approximate the person's shape and anatomical structure. A realistic appearance is achieved by color texture mapping from the multi-view images. Their approaches focus on the visualization result of human models. In our approach, a new deformation technique is developed, which has better continuity and local deformation properties. Lee et al. [6] also presented a method for full body cloning. Their system utilizes photos taken from the front, side and back of a person in any given imaging environment without requiring a special background or controlled illuminating condition. A seamless generic body specified in the VRML H-Anim 1.1 format [7] is used to generate an individualized virtual human. Their body-cloning component has two steps: 1) feature point specification, and 2) two-stage body modification by using feature points and body silhouette respectively. The feature points in their system should be specified interactively, they can be processed automatically in our approach by applying human knowledge based feature extraction.

In our virtual human modeling approach, an efficient segmentation method is applied on the two photographs to obtain the contours of the human body. Various algorithms are available for boundary extraction [8, 9, 10]. The active contour model can be considered as an energy-minimizing approach, it searches for the local energy minimum on a potential surface. We would like to give special consideration to a relatively new approach [10], which can detect objects whose boundaries are not necessarily defined by the gradient method. However, this approach is very time-consuming. In this paper, we build a pyramid for the given photograph and perform a multi-resolution segmentation, which accelerates the silhouette extraction process.

After the contour of a human model is extracted from the photographs, the features on the human contours are extracted by human morphology rules. The silhouettes with features defined are the input of our deformation. We use the reference silhouettes (the front-view and right-view silhouettes of the template human

model) and the target silhouettes (the front-view and right-view silhouettes of the human from the photographs) to deform the template human model (which is represented by a polygonal mesh) to construct a new human model. The modeling and animation of deformable objects have been an active area of research for a long time. Free-form deformations (FFDs) [11] and their variants [12, 13, 14, 15] are popular and provide a high level of geometric control over the deformation. FFDs are useful for coarse-scale deformations but inadequate for finer-scale deformations, even if a very dense lattice or customized lattice shape is defined. Axial deformation [16] provides a more compact representation in which a line segment or a curve is used to define an implicit global deformation. Our deformation technique appears to have better continuity and local deformation properties with reference to the warping [17] and the wire deformation [18].

3. Silhouette from Photograph

We determine the silhouette of human models from photographs by the segmentation technique. Our segmentation model is related to the Chan-Vese algorithm [10]. To reduce the computing time needed to reach a stable result, we improve the Chan-Vese model by using the segmentation algorithm in the multi-pyramid levels. Computation is reduced because we can represent large-scale photographs in a more compact manner by fewer pixels at a lower resolution.

Basic idea

Before we describe our segmentation model, the symbols used are introduced in Table 1.

Table 1 Notations for segmentation

Symbol	Meaning
$g_0(x, y)$	The given image
Ψ	The bounded region defined by the active contour
$\Omega = \partial\Psi$	The boundary of Ψ - a variable curve
$\gamma(x, y)$	The level set function
$H(z)$	The Heaviside function
$\delta(z) = \frac{d}{dz} H(z)$	The delta function
c_1	The average of g_0 inside Ω (depending on Ω)
c_2	The average of g_0 outside Ω (depending on Ω)

Our segmentation model is based on the level set function and the Chan-Vese energy function [10]. New implicit representations [19] have been proposed based on the level set methods [20] for the image segmentation. The level set function $\gamma(x, y)$ is defined as:

$$\gamma(x, y) = \begin{cases} > 0 & (x, y) \in \Psi \\ < 0 & (x, y) \in \overline{\Psi} - \partial\Psi \\ = 0 & (x, y) \in \partial\Psi \end{cases} \quad (1)$$

where $\overline{\Psi}$ represents the region outside Ψ, and $\partial\Psi$ represents the boundary of Ψ. The energy function is based on the Mumford-Shah variational model [21] that captures the "most general" segmentation energy, which can be represented by the following equation,

$$E_{snake}(\Omega) = E_{inside}(\Omega) + E_{outside}(\Omega) = \mu Length(\Omega) + \lambda_1 \int_{inside(\Omega)} |g_0 - c_1|^2 dx + \lambda_2 \int_{outside(\Omega)} |g_0 - c_2|^2 dx \quad (2)$$

where μ is a relax factor of the length constraint, λ_1 is the ratio of the internal energy, and λ_2 is the ratio of the external energy. They are used to adjust the segmentation result [10]. Usually, we use $\mu = 0.05$, $\lambda_1 = 0.5 \sim 3.0$, and $\lambda_2 = 0.5 \sim 3.0$. For the level set formulation of the variation active contour model, the unknown variable Ω can be replaced by the unknown variable $\gamma(x, y)$. The slightly regularized version of the functions $H(z)$ and $\delta(z)$ is used to solve the associated Euler-Lagrange equation for the unknown function $\gamma(x, y)$. After integrating with the level set function, we can rewrite the energy function as $E_{snake}(\gamma, c_1, c_2)$ in the following way,

$$E_{snake}(\gamma, c_1, c_2) = \mu \iint_{\Psi} |\nabla H(\gamma)| dxdy + \lambda_1 \cdot \iint_{\Psi} |u_0 - c_1|^2 H(\gamma) dxdy + \lambda_2 \cdot \iint_{\Psi} |u_0 - c_2|^2 (1 - H(\gamma)) dx . \quad (3)$$

The unknown constants (c_1 and c_2) are explicitly represented as functions of $\gamma(x, y)$. Therefore, we only need to consider γ in the new representation of the energy – $E_{snake}(\gamma, c_1(\gamma), c_2(\gamma))$, where c_1, c_2 are fixed. $E_{snake}(\gamma, c_1(\gamma), c_2(\gamma))$ is minimized with respect to $\gamma(x, y)$, and τ is chosen as a test function of the same type of $\gamma(x, y)$, so we obtain

$$\lim_{t \to 0} \frac{1}{t} \left(E(\gamma + t\tau, c_1(\gamma), c_2(\gamma)) - E(\gamma, c_1(\gamma), c_2(\gamma)) \right) \quad (4)$$

which leads to

$$\frac{\partial \gamma}{\partial t} = \delta_\varepsilon(\gamma) [\left(\mu \int_{\Psi} \delta(\gamma) |\nabla \gamma| d\Psi \right) \cdot div \left(\frac{\nabla \gamma}{|\nabla \gamma|} \right) - \lambda_1 (g_0 - c_1)^2 + \lambda_2 (g_0 - c_2)^2] \quad (5)$$

in Ω. Since $\frac{\partial \gamma}{\partial t} = \frac{\gamma^{n+1} - \gamma^n}{\Delta t}$, by solving the above partial differential equations, we obtain γ^{n+1}. Then, instead of evolving the curve Ω, we consider the evolution of the level set function $\gamma(x, y)$ and extract the zero level to see the results.

Numerical solution

A finite difference method is applied to solve equation (5). Let (x_i, y_j) be the grid points, so $\gamma_{i,j}^n = \gamma(n\Delta t, x_i, y_j)$ approximates $\gamma(t, x, y)$, where $n \geq 0$. Discrete the equation (5) by

$$\Delta_-^x\gamma_{i,j}=\gamma_{i,j}-\gamma_{i-1,j},\ \Delta_+^x\gamma_{i,j}=\gamma_{i+1,j}-\gamma_{i,j},\Delta_-^y\gamma_{i,j}=\gamma_{i,j}-\gamma_{i,j-1},\ \Delta_+^y\gamma_{i,j}=\gamma_{i,j+1}-\gamma_{i,j},$$

we obtain

$$\begin{aligned}\frac{\gamma_{i,j}^{n+1}-\gamma_{i,j}^{n}}{\Delta t}=\delta\left(\gamma_{i,j}^{n}\right)\{\mu L\left(\gamma^{n}\right)\Delta_-^x(\frac{\Delta_+^x\gamma_{i,j}^{n+1}}{\sqrt{\left(\Delta_+^x\gamma_{i,j}^{n}\right)^2+\left(\gamma_{i,j+1}^{n}-\gamma_{i,j-1}^{n}\right)^2/4}})+\\ \mu L\left(\gamma^{n}\right)\Delta_-^y(\frac{\Delta_+^y\gamma_{i,j}^{n+1}}{\sqrt{\left(\gamma_{i+1,j}^{n}-\gamma_{i-1,j}^{n}\right)^2/4+\left(\Delta_+^y\gamma_{i,j}^{n}\right)^2}})-\lambda_1\left(u_{0,i,j}-c_1\left(\gamma^{n}\right)\right)^2+\lambda_2\left(u_{0,i,j}-c_2\left(\gamma^{n}\right)\right)^2]\end{aligned}\tag{6}$$

which can be converted into the following linear form

$$\begin{aligned}\gamma_{i,j}^{n+1}=\gamma_{i,j}^{n}+\Delta t\delta\left(\gamma_{i,j}^{n}\right)\{\mu L\left(\gamma^{n}\right)(C_1\gamma_{i+1,j}^{n+1}+C_2\gamma_{i-1,j}^{n+1}+C_3\gamma_{i,j+1}^{n+1}+C_4\gamma_{i,j-1}^{n+1}\\ -\frac{(C_1+C_2+C_3+C_4)}{\Delta t}\gamma_{i,j}^{n+1})-\lambda_1\left(u_{0,i,j}-c_1\left(\gamma^{n}\right)\right)^2+\lambda_2\left(u_{0,i,j}-c_2\left(\gamma^{n}\right)\right)^2]\end{aligned}\tag{7}$$

where

$$C_1=\frac{1}{\sqrt{\left(\gamma_{i+1,j}^{n}-\gamma_{i,j}^{n}\right)^2+\left(\gamma_{i,j+1}^{n}-\gamma_{i,j-1}^{n}\right)^2/4}},C_2=\frac{1}{\sqrt{\left(\gamma_{i,j}^{n}-\gamma_{i-1,j}^{n}\right)^2+\left(\gamma_{i-1,j}^{n}-\gamma_{i-1,j-1}^{n}\right)^2/4}},$$
$$C_3=\frac{1}{\sqrt{\left(\gamma_{i+1,j}^{n}-\gamma_{i-1,j}^{n}\right)^2/4+\left(\gamma_{i,j+1}^{n}-\gamma_{i,j}^{n}\right)^2}},C_4=\frac{1}{\sqrt{\left(\gamma_{i+1,j}^{n}-\gamma_{i-1,j-1}^{n}\right)^2/4+\left(\gamma_{i,j}^{n}-\gamma_{i,j-1}^{n}\right)^2}}.$$

The length term $\int_\Psi\delta(\gamma)|\nabla\gamma|d\Psi$ of equation (5) is converted to $L\left(\gamma^{n}\right)$ in equation (7), which is computed by the following equation after discretization.

$$L\left(\gamma^{n}\right)=Length\{\gamma^{n}=0\}=\sum_{i=0}^{m\_width}\sum_{j=0}^{m\_height}\delta\left(\gamma_{i,j}^{n}\right)\sqrt{\left(\frac{\gamma_{i+1,j}+\gamma_{i-1,j}}{2}\right)^2+\left(\frac{\gamma_{i,j+1}+\gamma_{i,j-1}}{2}\right)^2}\tag{8}$$

Applying equation (7) on an image, the active contour moves towards the boundary of the image object to be extracted. When $\frac{\left|\gamma_{i,j}^{n+1}-\gamma_{i,j}^{n}\right|}{\left|\gamma_{i,j}^{n}\right|}<\varepsilon$ (where ε is a small constant, e.g., $\varepsilon=0.005\%$), the iteration stops.

Improvement by multi-pyramid approach

Above single level segmentation algorithm obtains good results of interested object. However, the algorithm takes a long time to reach a stable result, especially for a large-scale photograph. To overcome this problem, we use multi-pyramid level segmentation. The computing time can be significantly reduced for we can represent the photograph in a more compact way by fewer pixels at a lower resolution. As shown in Fig. 2, the grids represent pixels of the given image, and the gray block represents the “pixel” used in a specified pyramid level. When we segment an image, we usually begin at a lower resolution pyramid level. Therefore, we can quickly get the rough boundary of the object to be segmented in the given image. After that, we use this rough

boundary as the initial condition of the segmentation in the next pyramid level to obtain a more accurate result. Thus, the whole procedure of segmentation is speed up.

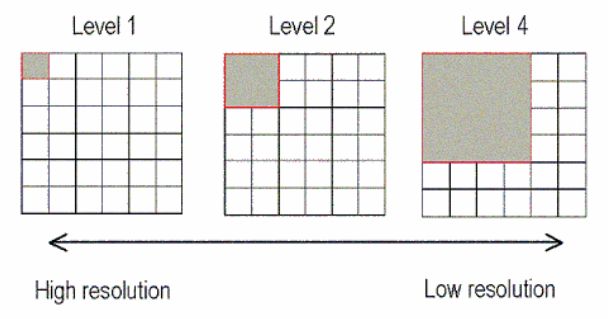

Fig. 2 Computing nodes in multi-pyramid level segmentation

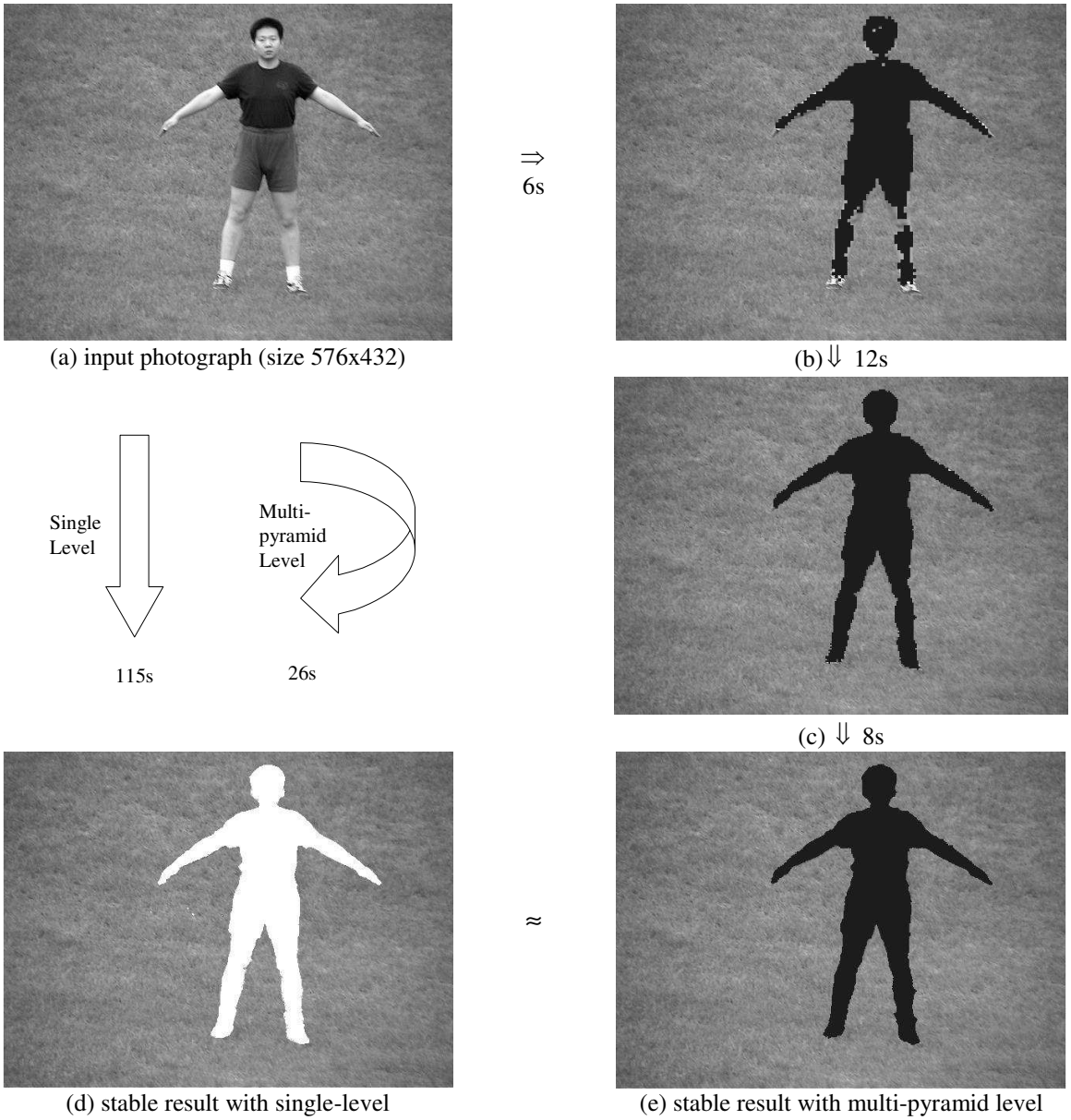

(a) input photograph (size 576x432)

(b)

(c)

(d) stable result with single-level

(e) stable result with multi-pyramid level

Fig. 3 Single level segmentation vs. multi-pyramid level segmentation

The comparison between single level segmentation and multi-pyramid level segmentation is given in Fig. 3. Fig. 3a has 576x432 pixels. After applying the single level segmentation algorithm on Fig. 3a, it takes 115s to obtain a stable result (shown in Fig. 3d). The flow of multi-pyramid level segmentation is shown in Fig. 3a, 3b, 3c, and 3e. Fig. 3a is segmented with 3 pyramid levels and the resultant quality is equal to that generated with a single level. But the computing cost is dramatically reduced. It takes only 26 seconds to obtain a stable result (The testing is performed on a PIII 500MHz PC with 128MB RAM). The pixels on the boundary of Ω are detected by searching the points with $\gamma = 0$. It is straightforward.

4. Feature Extraction

The objective of feature extraction is to establish the correct correspondence between the silhouette of the photograph and the silhouette of the synthetic model. We should robustly extract a set of feature points for a wide range of changes in the body shape and size. To achieve this, we assume that the person stands approximately in a pre-specified posture and wears tight clothes so that both the armpits and the crotch are visible. Before the feature extraction, we specify the coordinate system of the silhouettes in the front view and the right view as shown in Fig. 4. The human model faces along the *x*-axis direction, the *y*-axis is horizontally pointing to the left of the human model, and the *z*-axis is vertically pointing upwards. Several key feature points are defined in the silhouette (see Fig. 4). The proportion from the key feature points can obtain other auxiliary feature points, which is very straightforward. Thus, we focus on the extraction of the key feature points here.

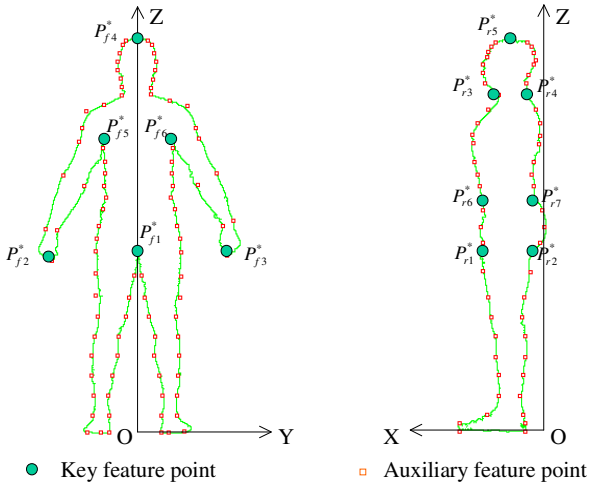

Fig. 4 Coordinate system of the silhouettes

Some notations need to be defined before feature extraction is explained. The total number of points on silhouette Ω is defined by N_P; Ω_f represents the silhouette obtained from the front view, and Ω_r represents the silhouette obtained from the right view; the numbers of points on Ω_f and Ω_r are N_P^f and N_P^r. $X(P_i)$,

$Y(P_i)$, and $Z(P_i)$ represent the X, Y, and Z coordinate of point P_i on Ω. We assume that the points on Ω_f and Ω_r are sorted in an anti-clockwise order, $\Gamma_+(P_i,\Omega)$ represents the set of points that comes after point P_i along Ω, and $\Gamma_-(P_i,\Omega)$ represents the set of points that comes before point P_i along Ω.

Before the extraction, we scale and translate the coordinate system to the position and orientation shown in Fig. 4, where the Z coordinates of the two views are the same. The scaling is calibrated by the height of the human body. An algorithm for extracting feature points from Ω_f and Ω_r is given below.

1. Key feature extraction from front view (find points P^*_{f1-f6}):

Defining the maximum value and the minimum value of $Y(P_i)$ and $Z(P_i)$ ($P_i \in \Omega_f$) as $Y_{\max}$, $Y_{\min}$ and $Z_{\max}$, $Z_{\min}$, we use the following steps to obtain points P^*_{f1-f6}.

(a) P^*_{f1} is a point that satisfies the following conditions: $P^*_{f1} \in \Omega_1$, $Z(P^*_{f1}) > Z(\Gamma_+(P^*_{f1},\Omega_1))$, and $Z(P^*_{f1}) > Z(\Gamma_-(P^*_{f1},\Omega_1))$, where

$$\Omega_1 = \{P_i \mid P_i \in \Omega_f, Z(P_i) < (\frac{2}{3}Z_{\max} + \frac{1}{3}Z_{\min}), (\frac{1}{4}Y_{\max} + \frac{3}{4}Y_{\min}) < Y(P_i) < (\frac{3}{4}Y_{\max} + \frac{1}{4}Y_{\min})\};$$

(b) P^*_{f2} is a point that satisfies the following conditions: $P^*_{f2} \in \Omega_2$, $Z(P^*_{f2}) < Z(\Gamma_+(P^*_{f2},\Omega_2))$, and $Z(P^*_{f2}) < Z(\Gamma_-(P^*_{f2},\Omega_2))$, where $\Omega_2 = \{P_i \mid P_i \in \Omega_f, Y_{\min} < Y(P_i) < Y_{\min} + \frac{1}{4}(Y_{\max} - Y_{\min})\}$;

(c) P^*_{f3} is a point that satisfies the following conditions: $P^*_{f3} \in \Omega_3$, $Z(P^*_{f3}) < Z(\Gamma_+(P^*_{f3},\Omega_3))$, and $Z(P^*_{f3}) < Z(\Gamma_-(P^*_{f3},\Omega_3))$, where $\Omega_3 = \{P_i \mid P_i \in \Omega_f, Y_{\max} - \frac{1}{4}(Y_{\max} - Y_{\min}) < Y(P_i) < Y_{\max}\}$;

(d) $P^*_{f4} = \{y = Y(P^*_{f1})\} \cap \{P_i \mid P_i \in \Omega_f, Z(P_i) > (\frac{2}{3}Z_{\max} + \frac{1}{3}Z_{\min})\}$;

(e) P^*_{f5} is a point that satisfies the following conditions: $P^*_{f5} \in \Omega_5$, $Z(P^*_{f5}) > Z(\Gamma_+(P^*_{f5},\Omega_5))$, and $Z(P^*_{f5}) > Z(\Gamma_-(P^*_{f5},\Omega_5))$, where $\Omega_5 = \{P_i \mid P_i \in \Omega_f, f2 < i < f1\}$;

(f) P^*_{f6} is a point that satisfies the following conditions: $P^*_{f6} \in \Omega_6$, $Z(P^*_{f6}) > Z(\Gamma_+(P^*_{f6},\Omega_6))$, and $Z(P^*_{f6}) > Z(\Gamma_-(P^*_{f6},\Omega_6))$, where $\Omega_6 = \{P_i \mid P_i \in \Omega_f, f1 < i < f3\}$;

2. Key feature extraction from the right view (find points P^*_{r1-r7}):

The slope at point P_i is defined as $S(P_i)$. The maximum value and the minimum value of $X(P_i)$ and $Z(P_i)$ are represented by $X_{\max}$, $X_{\min}$ and $Z_{\max}$, $Z_{\min}$, where $P_i \in \Omega_r$.

(a) P_{r3}^* is a point satisfying the following conditions: $S(P_{r3}^*) = \max(S(P_i))$, $P_i \in \Omega_7$, and $P_{r3}^* \in \Omega_7$, where $\Omega_7 = \{P_i \mid P_i \in \Omega_r, Z(P_i) > (\frac{2}{3}Z_{\max} + \frac{1}{3}Z_{\min}), X(P_i) > \frac{1}{2}(X_{\max} + X_{\min})\}$;

(b) $P_{r4}^* = \{Z = Z(P_{r3}^*)\} \cap \overline{\Omega}_7$;

(c) $P_{r5}^* = \{X = \frac{1}{2}(X(P_{r3}^*) + X(P_{r4}^*))\} \cap \{P_i \mid P_i \in \Omega_r, Z(P_i) > (\frac{2}{3}Z_{\max} + \frac{1}{3}Z_{\min})\}$;

(d) $P_{r1}^* = \{Z = Z(P_{f1}^*)\} \cap \Omega_8$, $P_{r2}^* = \{Z = Z(P_{f1}^*)\} \cap \overline{\Omega}_8$, $P_{r6}^* = \{Z = Z(P_{f1}^*) + D\} \cap \Omega_8$, and $P_{r7}^* = \{Z = Z(P_{f1}^*) + D\} \cap \overline{\Omega}_8$, where $\Omega_8 = \{P_i \mid P_i \in \Omega_r, X(P_i) > X(P_{r5}^*)\}$, and $D = Z(P_{r5}^*) - Z(P_{r3}^*)$.

After applying the above rules on the silhouette obtained in section 3, all the key feature points can be extracted. The assistant feature points are computed by proportion rules used in the fashion industry [22, 23, 24]. Each feature points on the silhouette of the human model in photographs have a corresponding point on the silhouette of the template human model. In the next section, we use this correspondence to deform the template model to the shapes of the human models in the photographs.

5. View-dependent Deformation

With our method, the reference silhouettes (the front-view and right-view silhouettes of the synthetic human model) and the target silhouettes (the front-view and right-view silhouettes of the human from the photographs) are used to modify the template human model represented by a polygonal mesh. The system moves the vertices of the polygonal model so that the spatial relation between the original positions and the reference silhouettes is identical to the relation between the resulting positions and the target silhouettes. The movement is perpendicular to the view direction, and vertices do not move in the view direction. Thus, it is called view-dependent deformation. Our method is related to axial deformation [16]. The self-intersection problem of the axial deformation is solved in our approach, and the local deformation property is added.

Deformation

For a given point p in the view-dependent space of the object Φ, we want to find its corresponding point q related to the target curve. Firstly, the nearest point $R(u)$ to p on the reference curve is determined (If there is more than one point with a minimum distance, Lazarus et al. [16] define u to be the parameter with the smallest value). Two coordinate systems: one on the reference curve and the other on the target curve are

defined with u (Fig. 5). The reference curve coordinate system has its origin at $R(u)$, and $\hat{x}_r(u)$ is given by the tangent of R at u. Likewise, the target curve coordinate system has its origin at $T(u)$, and $\hat{x}_t(u)$ is given by the tangent of T at u. $\hat{y}_r(u)$ and $\hat{y}_t(u)$ can be determined by rotating $\hat{x}_r(u)$ and $\hat{x}_t(u)$ 90 degree in an anti-clockwise direction.

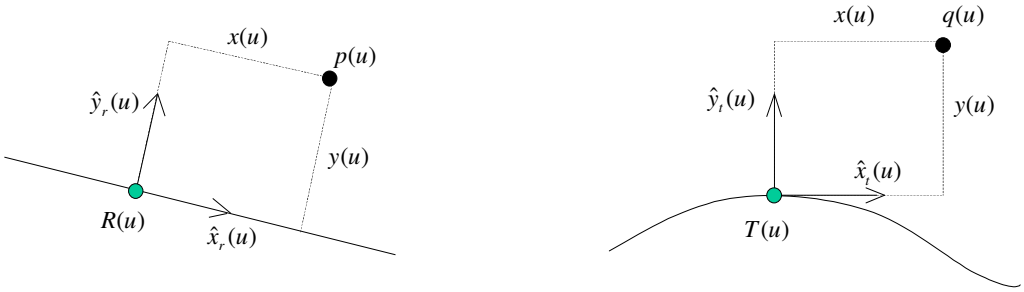

(a) reference curve **(b) target curve**

Fig. 5 Coordinate system for deformation

After defining the coordinate system, we can find the x and y coordinates of p in the reference curve coordinate system: $x(u) = (p - R(u)) \cdot \hat{x}_r(u)$ and $y(u) = (p - R(u)) \cdot \hat{y}_r(u)$. Next, we determine the point $q(u)$ corresponding to $p(u)$ by

$$q(u) = T(u) + x(u)\hat{x}_t(u) + y(u)\hat{y}_t(u) \tag{9}$$

This is the new location of $p(u)$ in our deformation.

Self-intersection problem

In cases of curves with a high curvature, self-intersection sometimes happens (see Fig. 6a and 6b, where the "horizontal" curve is the reference curve and the "bended" one is the target curve). In the human modeling, this always happens at the armhole during the deformation. Correa et al. (1998) [17] used weighted average of $q(u)$ for all u to avoid such a problem. With reference to the method of Correa et al., we use the following equation to determine the final coordinate of $q(u)$:

$$q = \frac{\sum_{i=1}^{n} c(u_i) q(u_i)}{\sum_{i=1}^{n} c(u_i)} \tag{10}$$

where $u_i = \frac{i - 0.5}{n}$, $i = 1, \ldots, n$. We want the contribution $c(u)$ to fall off with the growth of the distance $d(u)$ between the projected points of $p(u)$ and $R(u)$ in the view direction. Thus, we choose the contribution to be

$$c(u) = \frac{1}{\varepsilon + d(u)^f} \tag{11}$$

where ε is a small constant to avoid singularities when the distance is very close to zero, and f is a constant that controls how fast the contribution falls off with distance. In Fig. 6c, we use $\varepsilon = 10^{-6}$ and $f = 3$. The self-intersection problem is solved.

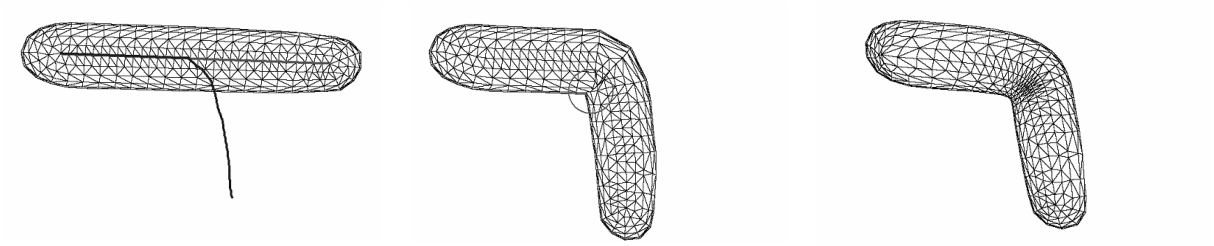

(a) high curvature **(b) self-intersection** **(c) result**

Fig. 6 Self-intersection problem

Deformation synthesis

In our virtual human modeling application, the synthetic human model needs to be synthesized from the deformation in both the view-dependent coordinate spaces of the front-view and the right-view. If, after transferring the coordinate, the final coordinate of $q(u)$ in the model space by the ith view-dependent deformation is $\hat{q}_i$, the final coordinate q^* of $q(u)$ in the model space is determined by taking the average,

$$q^* = \frac{1}{n}\sum_{i=0}^{n-1} \hat{q}_i \tag{12}$$

where n is the number of views ($n = 2$ in our system).

Influence area

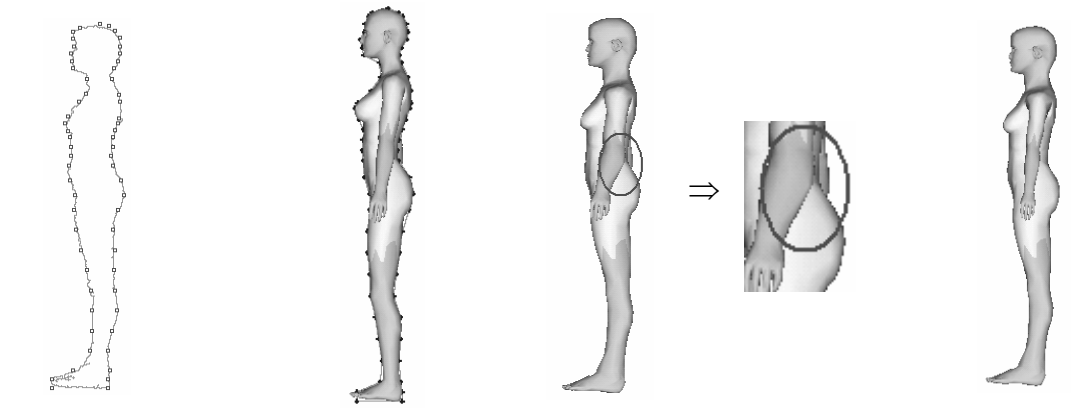

(a) silhouette **(b) template** **(c) global deform** **(d) local deform**

Fig. 7 Global vs. local deformation

After using equation (10) to calculate the deformed position of $q(u)$, obviously, the positions of all points on the original object Φ are changed (we call it global deformation). Such deformations sometimes do not follow users' expectation, i.e., when deforming the template human model in Fig. 7b to the silhouette in Fig. 7a, the deformation method of equation (10) leads to the distortion of the arms (Fig. 7c, inside the circle) for it is too close to the silhouette. This is not the intention of the users. Here, we introduce a parameter r, which can be used to define the influence area of the deformation to avoid this problem; the parameter r controls the deformation area through influencing the function $c(u)$. The new function $c(u)$ should satisfy the following three constraints:

Constraint 1 If $d(u) > r$, the function should be zero;

Constraint 2 The function should fall off with the growth of the distance function $d(u)$ when $d(u) \le r$, and it should be a single value function;

Constraint 3 The function should have a maximum value of 1 when $d(u) = 0$, and have a minimum value of 0 when $d(u) = r$ (C^0 continuity).

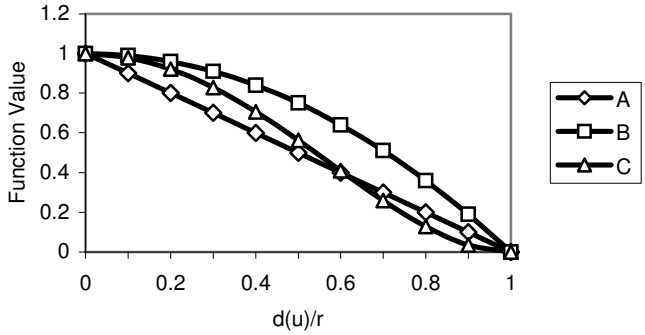

Fig. 8 Contribution function

It is clear that the following function satisfies the above constrains.

$$c(u) = \begin{cases} 1 - \dfrac{d(u)}{r}, & d(u) \le r \\ 0, & d(u) > r \end{cases} \tag{13}$$

The curve of the contribution function $c(u)$ in equation (13) is shown in Fig. 8 (curve A). To change the continuity at $d(u) = 0$ from C^0 to C^1, the contribution function is changed to

$$c(u) = \begin{cases} 1 - (\dfrac{d(u)}{r})^2, & d(u) \le r \\ 0, & d(u) > r \end{cases} \tag{14}$$

The curve of the contribution function $c(u)$ in equation (14) is shown in Fig. 8 (curve B). To change the continuity at $d(u) = r$ from C^0 to C^1, the contribution function is changed to

$$c(u) = \begin{cases} [(\frac{d(u)}{r})^2 - 1]^2, & d(u) \le r \\ 0, & d(u) > r \end{cases} \tag{15}$$

The curve of the contribution function $c(u)$ in equation (15) is shown in Fig. 8 (curve C). After applying the new representation of $c(u)$ above into equation (10), we can obtain a local deformation result (as shown in Fig. 7d) by using the distance between a feature point and the central axis in the front-view as $d(u)$, and using half of the shoulder width in the front-view as r.

A more accurate method is to get the contours on the arm separately from those on the body by segmentation; and then using these contours to get the arm's thickness. However, the garment industry does not care about the girth of arms very much [22, 23, 24]; so our approach is an acceptable solution.

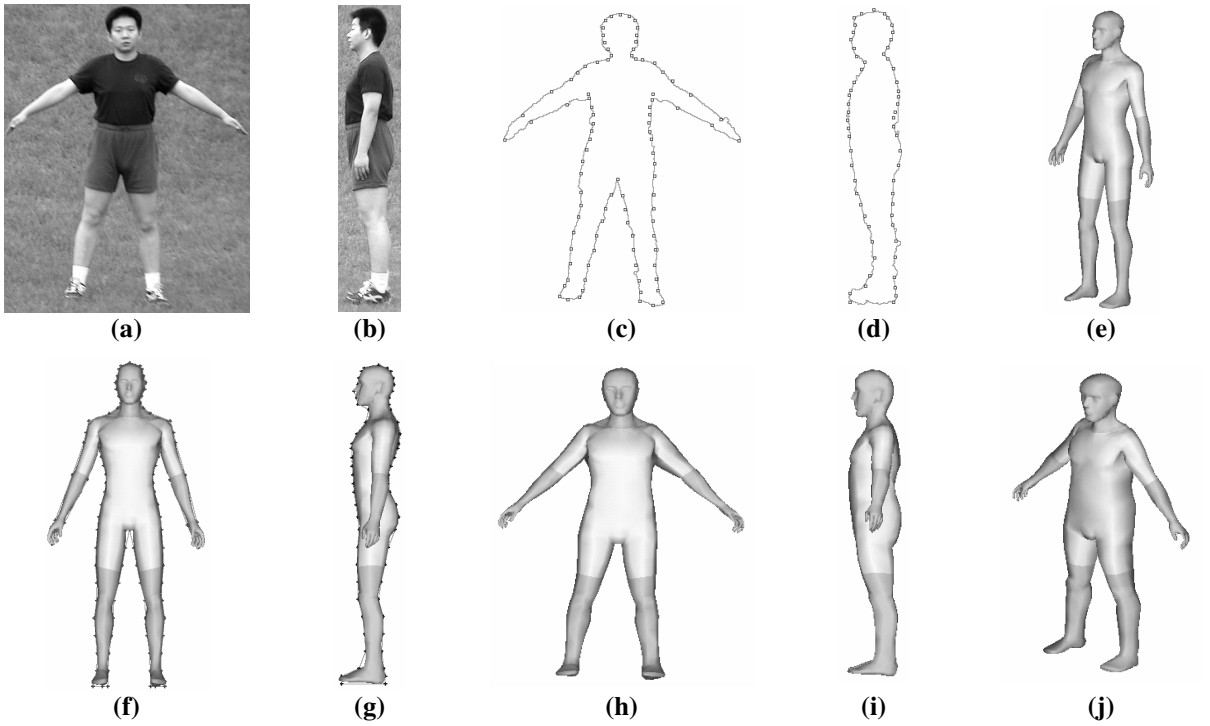

Fig. 9 Virtual human modeling

6. Result

The whole procedure of virtual human modeling is shown in Fig. 9, where Fig. 9a and 9b are the photographs of the front view and the right view of a human body wearing tight clothes, Fig. 9c and 9d show the contour of the human with feature extraction results, Fig. 9e is the template model, Fig. 9f and 9g show the contour of the template model with feature defined, Fig. 9h, 9i and 9j show the deformation results of our view-

dependent deformation technique. The result model has many applications in the garment industry. Fig. 10 shows the results of the other two examples.

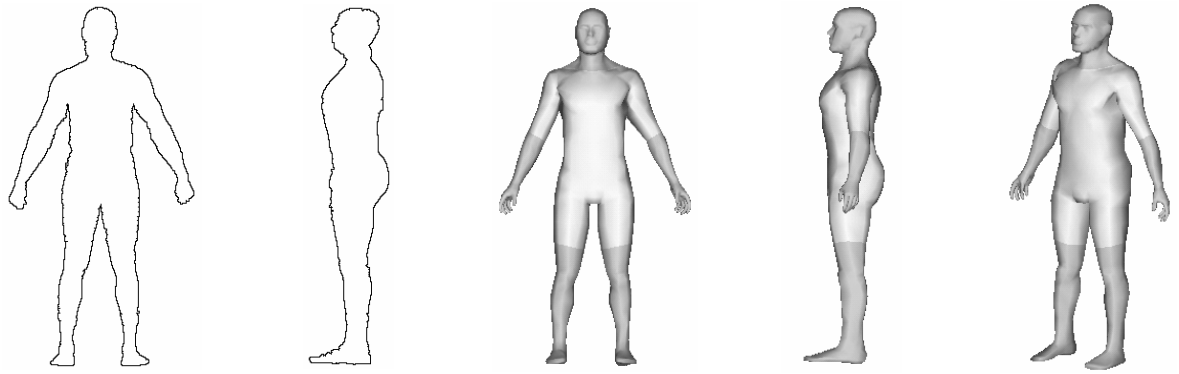

(a) example I: male model

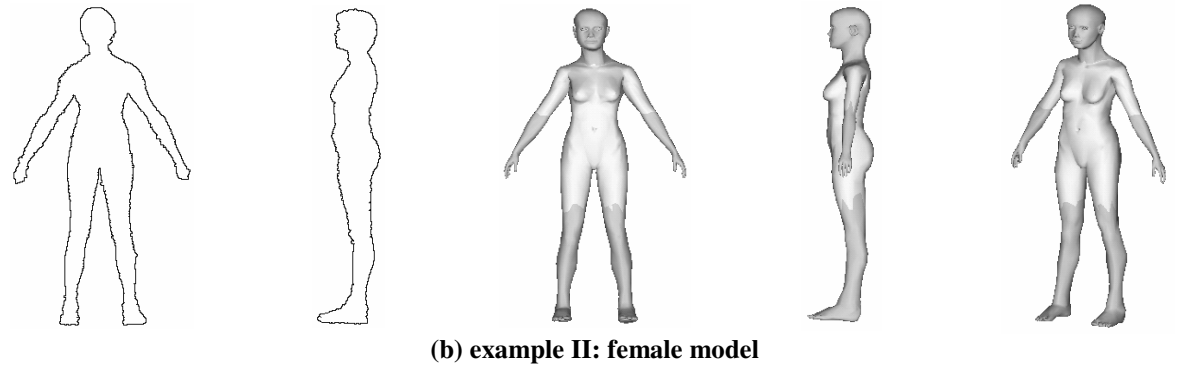

(b) example II: female model

Fig. 10 Results of two examples

7. Shape Approximation Error

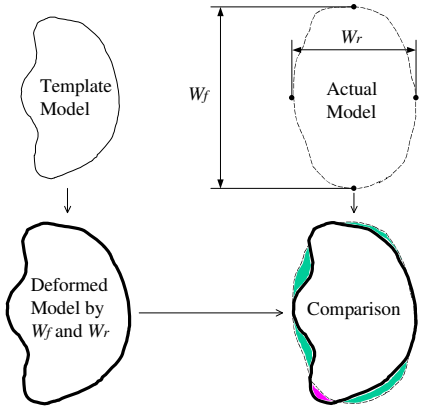

Fig. 11 Shape approximation error

In this paper, we deform the template model from the silhouettes of two orthogonal views: front-view and right-view, so the deformation gives an approximation error for the body surface (as shown in Fig. 11). Suppose the dash curve represents the horizontal cross-section of the actual model (W_f is the width in the front-view and W_r is the width in the right-view), the solid curve represents the horizontal cross-section of the template mode,

and the bolded curve represents the deformed curve, the shape approximation error is shown by comparing the cross-section of the deformed model and the cross-section of the actual model (the gray region shows the shape approximation error).

8. Applications

Some potential applications that might benefit from this technology are briefly introduced in this section. They are: 1) dimensions extraction for human models; 2) rapid prototyping for mannequin manufacturing; and 3) three dimensional garment construction.

Table 2 Selected key dimensions (unit: CM)

Dimensions	Male (Fig. 9)		Male (Fig. 10a)	Female (Fig. 10b)
Height	174.28	175*	180.01	171.86
Head Height	27.00	25	23.07	22.12
Belly Button	100.00	103	104.89	104.69
Crotch Depth	24.67	25	23.46	20.68
In-Seam	75.33	78	81.54	84.01
Knee Length	48.00	49	45.46	46.14
Vertical Truck	168.17	170	173.29	149.21
Half Shoulder Width	23.70	24	22.56	18.99
Arm Hole Circumference	35.75	36	37.07	31.00
Arm Length	56.48	58	60.04	54.01
Head Girth	68.22	64	62.58	66.09
Neck Girth	42.64	44	42.01	39.38
Chest	108.95	109	108.57	91.54
Lower Chest	103.07	103	102.21	75.46
Waist	102.14	102	93.53	74.27
Lower Waist	107.23	105	94.76	83.45
Hip/Seat	114.15	112	107.06	94.44
Lower Hip/Seat	114.23	112	110.41	96.98
Thigh Girth	71.15	69	73.02	62.14
Mid-thigh Girth	58.44	58	59.50	48.40
Knee Girth	45.27	45	38.50	33.74
Mid-calf Girth	41.86	43	39.90	35.61
Below-ankle Girth	36.33	35	35.29	37.75

* This column shows the tailor measurement result of the human body in Fig. 9.

Dimensions extraction

Since our virtual human model is deformed from the template human model, the features defined on the template are maintained during the deformation process. Thus, the dimensions of the human model in the photographs can be obtained easily from the feature lines maintained on the reconstructed human model (the feature lines are defined with reference to the rules in the fashion industry [22, 23, 24]). Table 2 shows the selected key dimensions of the reconstructed 3D models in Fig. 9 and 10, and Fig. 12 shows the human models with the feature lines. Studies have shown that about 40 to 50 measurements are required by pattern makers in the garment industry. Taking measurements manually is extremely boring work. Our method is a fast solution. By comparing the tailor measurement and the measurement from our 3D model (Table 2), we can say that the

result of our method is acceptable. The error mainly comes from the shape approximation error shown in section 7.

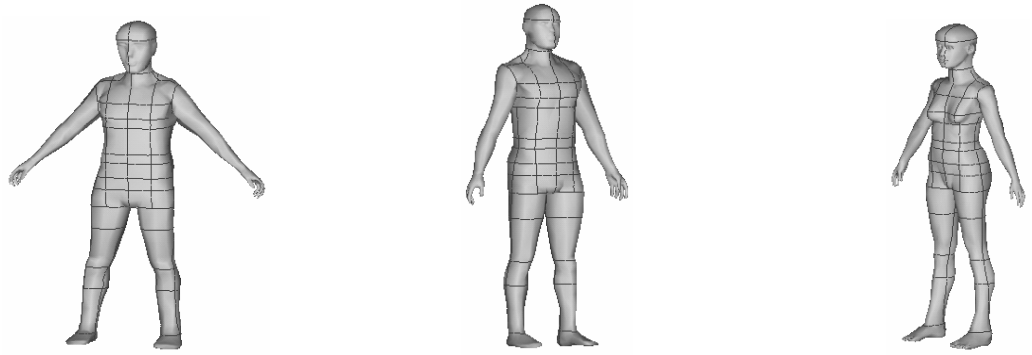

(a) **(b)** **(c)**

Fig. 12 Human models with feature lines

Rapid prototyping for mannequin manufacturing

In the garment industry, customized physical models are sometimes required. To produce a custom-made mannequin model, layered-manufacturing (LM) [25] has been adopted which builds the model layer by layer repeatedly. Since the stereolithography file (STL) is the standard input format of almost all RP systems (STL file represents geometry of objects by a facet model), and our system represents the human model by a triangular mesh, it is very easy to output the reconstructed human model to any rapid prototyping (RP) system from our system. Fig. 13 shows one example of a full-scaled custom mannequin model, where Fig. 13a shows the virtual mannequin model converted from the virtual human model shown in Fig. 10b, and Fig. 13b shows the manufactured result of the virtual mannequin model in Fig. 13a using LM.

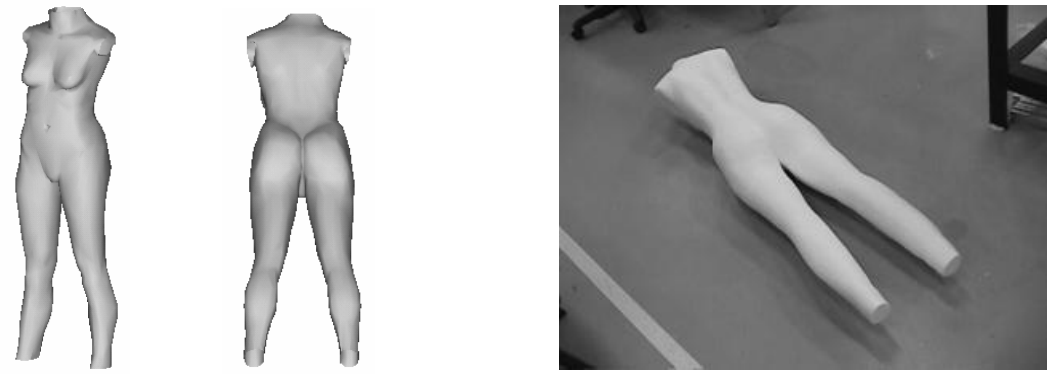

(a) mannequin from female model of Fig. 10b **(b) LM result**

Fig. 13 Full-scaled custom mannequin model using layered-manufacturing

Our virtual human modeling approach speeds up the procedure of designing geometrical mannequin models for rapid prototyping. Since only photographs from two orthogonal views are required, so our approach is very useful for building a remote or global rapid prototyping market manufactory for mannequin models.

Three-dimensional garment construction

The technique of virtual human modeling described in this paper serves as the foundation of a new technique that allows pattern designers to design patterns directly on a 3D human model with feature lines defined. Currently, the alternative technique only focuses on the simulation of a 3D dressing result, but not on the 3D design. Thus, it needs the 2D patterns as the input [26]. A demonstration of the new technique is shown in Fig. 14. This new technique gives pattern designers a tool to design patterns directly on the 3D human model according to the feature lines. For example, Fig. 14a shows the human model with feature lines defined and the 3D garment profile given by designers (bold curves); variational subdivision scheme [27, 28] is applied to the profile to construct a 3D surface to interpolate the profile (Fig. 14b); Fig. 14c and 14d are the draping results of a skirt. We found that the garment constructed by this new technique fits the human model nicely.

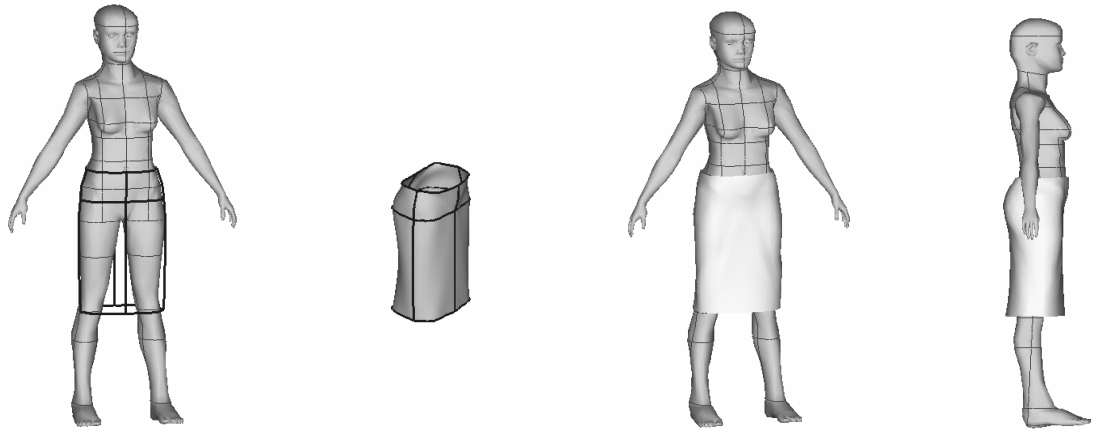

(a) **(b)** **(c)** **(d)**

Fig. 14 Examples of three-dimensional garment construction

9. Conclusion and Discussion

The paper describes the development of a technique of virtual human modeling for the garment industry using two photographs of a human body from two specific views. Our demo system is implemented on Windows NT/2000, using Visual C++ and OpenGL Library (The interface of our demo system is shown in Fig. 15). The whole procedure consists of three steps: 1) apply an efficient segmentation method to obtain the silhouette of a human model from two photographs; 2) extract the feature points on the silhouette of the human model; and 3) deform the template human model according to the silhouette with feature points. Compared with earlier approaches, our method has the following advantages:

- The speed of human model construction is increased since the speed of contour extraction is increased.
- The feature points on the silhouette are extracted automatically by human morphology rules.

- Our method is based on a view-dependent deformation technique, so the features defined on template human models are maintained, which can benefit post-applications.
- Mumford-Shah segmentation, which is little influenced by noise, is applied to photographs to obtain the contours of a human model; and it is accelerated by applying multi-pyramid levels during the segmentation process.
- A new deformation technique related to the axial deformation is derived, and the self-intersection problem in axial deformation is solved in our deformation approach, and a local deformation parameter is added. Thus, our deformation technique appears to have good continuity and local deformation properties.

At the end of the paper, in order to demonstrate the functionality of the virtual human model, three potential applications in the garment industry are given.

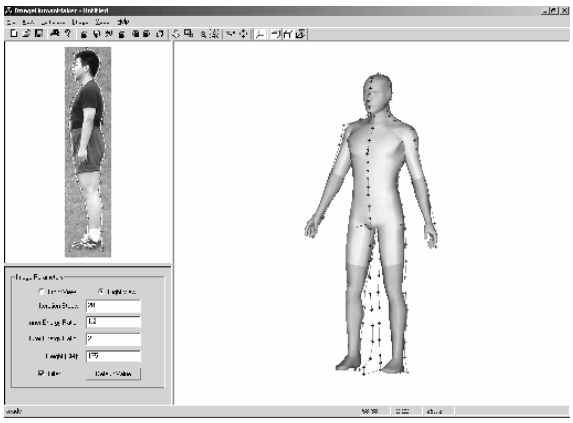

Fig. 15 Interface of our demo system

The limitation of our virtual human construction approach is the shape approximation error. Further research can focus on how to overcome the limitation by adding more silhouettes from other specified views (e.g., the view where the viewing direction is between the directions of the front-view and the right-view) or by applying human intelligence on the algorithm.

Acknowledgement

The authors would like to acknowledge the comments given by Mr. Luo Zegang and Mr. Danny Cheung, and the support from the Hong Kong Research Grant Council project: "HKUST6164/98E: Feature-based optimized tool path for layered manufacturing" and the CAD/CAM Facility of the Hong Kong University of Science and Technology.

References

[1] Au C.K., and Yuen M.M.F., Feature-based reserve engineering of mannequin for garment design. Computer Aided Design, 1999, 31(12): 751-759.

[2] Fischer A., and Park S., Remote sensing and LOD modeling for manufacturing products. International Journal of Advanced Manufacturing and Technology, pp. 91-94, 1998.

[3] Varady T., Martin R. R., and Cox J., Reverse engineering of geometry models – an introduction. Computer Aided Design, 1997, 29(4): 255-268.

[4] Hoppe H., DeRose T., Duchamp T., Halstead M., Jin H., McDonald J., Schweitzer J., and Stuetzle W., Piecewise smooth surface reconstruction. SIGGRAPH 94 Conference Proceedings, 1994, pp.295-302.

[5] Hilton A., Beresford D., Gentils T., Smith R., Sun W., Illingworth J., Whole-body modelling of people from multiview images to populate virtual worlds. Visual Computer, 2000, 16(7): 411-36. Publisher: Springer-Verlag, Germany.

[6] Lee W., Gu J., and Magnenat-Thalmann N., Generating animatable 3D virtual humans from photographs. Computer Graphics Forum, vol.19, no.3, 2000, pp.1-10, UK.

[7] VRML Humanoid Animation Working Group, H-Anim 1.1 Specification. http://h-anim.org.

[8] Kass M., Witkin A., and Terzopoulos D., Snake: Active contour models. International Journal of Computer Vision, vol.1, no.4, 1988, pp.321-331, Netherlands.

[9] Caselles V., Catte F., Coll T., and Dibos F., A geometric model for active contours in image processing. Numerische Mathematik, vol.66, no.1, 1993, pp.1-31, Germany.

[10] Chan T.F., and Vese L.A., Active contours without edges. IEEE Transactions of Image Processing, vol.10, no.2, Feb. 2001, pp.266-277, USA.

[11] Sederberg T., and Parry S., Free-form deformations of solid geometric models. Computer Graphics, vol. 20, 1986, pp.151-160.

[12] Coquillart S., Extended free-form deformations: A sculpting tool for 3D geometric modeling. Computer Graphics, vol. 24, no. 4, 1990, pp.187-196.

[13] Hsu W., Hughes J., and Kaufmann H., Direct manipulations of free-form deformations. Computer Graphics, vol. 26, no. 2, 1992, pp.177-184.

[14] Chang Y.K., and Rockwood A.P., A generalized de Casteljau approach to 3D free-form deformation. Computer Graphics, vol. 28, no.4, 1994, pp.257-260.

[15] MacCracken R., and Joy K., Free-form deformations with lattices of arbitrary topology. SIGGRAPH 96 Conference Proceedings, New Orleans, Louisiana, USA, 1996, pp.181-189.

[16] Lazarus F., Coquillart S., and Jancene P., Axial deformations: an intuitive deformation technique. Computer-Aided Design, vol. 26, no. 8, 1994, pp.607-613.

[17] Correa W.T., Jensen R.J., Thayer C.E., and Finkelstein A., Texture mapping for cel animation. SIGGRAPH 98 Conference Proceedings, Orlando, Florida, USA, 1998, pp.435-456.

[18] Singh K., and Fiume E., Wires: a geometric deformation technique. SIGGRAPH 98 Conference Proceedings, Orlando, Florida, USA, 1998, pp.405-414.

[19] Adelson E.H., and Weiss Y., A unified mixture framework for motion segmentation: incorporating spatial coherence and estimating the number of models. Computer Vision and Pattern Recognition Conference Proceeding, San Francisco, USA, 1996, pp.321-326.

[20] Osher S., and Sethian J.A., Fronts propagating with curvature dependent speed: Algorithms based on Hamilon – Jaoobi Formulation. Journal of Computational physics, vol. 76, 1988, pp.12-49.

[21] Mumford D., and Shah J., Optimal approximation by piecewise smooth functions and associated variational problems. Communications on Pure and Applied Mathematics, vol. 42, 1989, pp.577-685.

[22] Solinger J., Apparel manufacturing handbook: analysis, principles, and practice. Publisher: Columbia, S.C.: Bobbin Media Corp., 1988.

[23] Taylor P.J., and Shoben M.M., Grading for the fashion industry: the theory and practice. Publisher: Cheltenham, England Thornes, 1990.

[24] Cooklin G., Pattern grading for women's clothes: the technology of sizing. Publisher: Oxford : BSP Professional Books, 1990.

[25] Chang T.K.K., Feature-based modeling and manufacturing of sculpture object. Thesis for Mechanical Engineering Department of the Hong Kong University of Science and Technology, 1998, Hong Kong.

[26] Fan J., Wang Q.F., Chen S.F., Yuen M.M.F. and Chan C.C., A spring-mass model-based approach for warping cloth patterns on 3D objects. The Journal of Visualization and Computer Animation, Vol. 9 No. 4, October/December 1998, pp. 215-227.

[27] Kobbelt L., Discrete fairing and variational subdivision for freeform surface design. The Visual Computer, vol.16, no.3-4, 2000, pp.142-158. Publisher: Springer-Verlag, Germany.

[28] Kobbelt L., Discrete Fairing. Proceeding of the Seventh IMA Conference on the Mathematics of Surfaces' 97, 1997, pp.101-131.